Int J Adv Manuf Technol (2014) 74:341–349
DOI 10.1007/s00170-014-6004-3

ORIGINAL ARTICLE

Modeling of the static tool influence function of bonnet polishing based on FEA

C. Wang · Z. Wang · X. Yang · Z. Sun · Y. Peng · Y. Guo · Q. Xu

Received: 18 November 2013 / Accepted: 23 May 2014 / Published online: 1 June 2014

Abstract The purpose of this paper is to investigate the model of the static tool influence function (sTIF) of bonnet polishing (BP). Three kinds of sTIF are mathematically modeled, which are static tool influence function of tilted polishing ($sTIF_t$), static tool influence function of discrete precession polishing ($sTIF_d$), and static tool influence function of continuous precession ($sTIF_c$), respectively. Pressure distribution in the contact area is confirmed based on finite element analysis (FEA) technology. A group of experiments to extract the polishing spots have been conducted to verify the accuracy of the sTIF model. Meanwhile, the difference between $sTIF_d$ and $sTIF_c$ is studied. It turns out that the removal depths of $sTIF_d$ and $sTIF_c$ are almost the same, and the continuous precession polishing can be replaced by discrete precession polishing to ease control in practical polishing process especially for the aspheric surfaces polishing.

Keywords Tool influence function · FEA · Bonnet polishing · Pressure distribution

Electronic supplementary material The online version of this article (doi:10.1007/s00170-014-6004-3) contains supplementary material, which is available to authorized users.

C. Wang (✉) · Z. Wang · X. Yang · Z. Sun · Y. Peng · Y. Guo
Department of Mechanical and Electrical Engineering, Xiamen University, Xiamen 361005, China
e-mail: wcj-2000@163.com

Z. Wang
e-mail: wangzhenzhong@xmu.edu.cn

X. Yang
e-mail: yxcrab@163.com

Z. Sun
e-mail: devinszj@163.com

Y. Peng
e-mail: pengyf@xmu.edu.cn

Y. Guo
e-mail: guoyb@xmu.edu.cn

C. Wang · Q. Xu
Research Center of Laser Fusion, China Academy of Engineering Physics, Mianyang 621900, China

Q. Xu
e-mail: xuqiao@vip.sina.com

Nomenclature

sTIF	Static tool influence function
$sTIF_c$	Static tool influence function of continuous precession polishing
$sTIF_d$	Static tool influence function of discrete precession polishing
$sTIF_t$	Static tool influence function of tilted polishing
k	Removal coefficient
p	Polishing pressure
v	Relative speed between the tool and the workpiece
v_r	Velocity of point Q derived from the rotation of H-axis
v_p	Velocity of point Q derived from the rotation of A-axis
v_Q	Total relative speed of point Q
ω_1	Rotation speed of H-axis
ω_2	Rotation speed of A-axis
l	Z offset of the bonnet
R	Bonnet radius
p_s	Pressure distribution in the contact area
p_{max}	The maximum pressure in the contact area
λ	Distance from one of the point in the contact area to the center
σ	Standard deviation
φ	Modification coefficient

1 Introduction

Bonnet polishing (BP) combined with precession movement, developed by Zeeko Ltd in collaboration with the Optical Science Laboratory at University College London and Loh

Optikmaschinen, is a novel precision polishing process especially for aspheric or free-form surface [1, 2]. It uses a rotating and inflated spherical membrane tool (the "bonnet"), which naturally molds itself to the local aspheric surface. A wide range of surface contact area can be achieved between the tool and the workpiece by changing the tool pressure. The bonnet polishing technology have shown its flexible tooling ability and been demonstrated to achieve excellent surface finishing accuracy when aided with a precision CNC capability and the built-in process intelligence [3–6].

BP is a member of deterministic polishing, such as computer-controlled optical surfacing (CCOS) [7], ion beam figuring (IBF) [8, 9], magnetorheological finishing (MRF) [10, 11], fluid jet polishing (FJP) [12–14], etc. The material removal function of deterministic polishing can be expressed as two-dimensional convolution of tool influence function (TIF) and dwell time function [15]. Hence, the final surface of deterministic polishing could be predicted and designed by controlling the dwell time. Therefore, the modeling of TIF is important. Jones [7] proposed the theoretical TIF of CCOS by assuming uniform pressure and orbital velocity and optimized the process by computer simulations. Jiao [9] built the model to relate the property factors, such as material removal efficiency, disturbance depth and thermal effect, and process parameters of the ion beam figuring based on the Sigmund sputtering theory. Dai et al. [10] established a calibrated and predictive TIF model of MRF, which can be used to accurately predict the removal function of a workpiece to be polished whose material is different from the spot part. Lin [16] developed an analytical model to describe the relationship between polishing parameters and TIF, which has been verified experimentally. Yi et al. [17] proposed a new computational technique called KTIF to increase the predictability of material removal in pitch tool-based surface figuring, which has been proven to have superior prediction performance.

Studies on TIF of BP also have been reported. Walker et al. [3] demonstrated the experimental TIF but not modeled it mathematically. Kim et al. [18] presented a theoretical model of static tool influence function (sTIF) for efficient fabrication of 2 m class hexagonal segment mirrors for ELT projects. However, its pressure distribution is derived from the reverse computation of the actual TIF, which means that the measuring of actual TIF is the premise to generating the mathematical TIF model. It is inconvenient for the process practically.

In this paper, a new computational technique to model the sTIF was proposed. The pressure distribution in the contact area was achieved using FEA method. Combining with three kinds of movement of the polishing tool which are tilted polishing, discrete precession polishing, and continuous precession polishing, all of their TIFs were modeled and demonstrated. Experiments have been conducted to generate the sTIF to verify the simulation model.

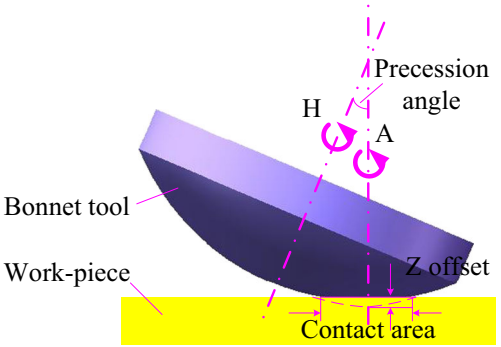

Fig. 1 Polishing model of BP

2 Modeling and simulation of sTIF

BP adopts a unique precession movement mode. The rotation axis of the tool is tilted to the surface's local normal, at an angle of typically 10–25° (called "precession angle") [3]. Figure 1 shows the polishing model of BP. The size of the contact area is controlled by Z offset between the bonnet tool and the workpiece.

sTIF is the removal function generated without considering the effect of the feed rate. According to the well-known Preston's law, the material removal function can be expressed as follows:

$$\frac{\mathrm{d}z}{\mathrm{d}t} = kpv \tag{1}$$

where dt is the dwell time, dz is the material removal during the dwell time, k is removal coefficient, p is the polishing pressure, and v is the relative speed between the tool and the workpiece.

2.1 Modeling of the polishing velocity

In order to determine polishing velocity in the contact area, the schematic diagram of the precession bonnet tool is built in Fig. 2. Q is a point in the contact area, v_r is the velocity of point Q derived from the rotation of H-axis, v_p is the velocity of point Q derived from the rotation of A-axis, ω_1 is the rotation speed of H-axis, ω_2 is the rotation speed of A-axis, O_1 is the

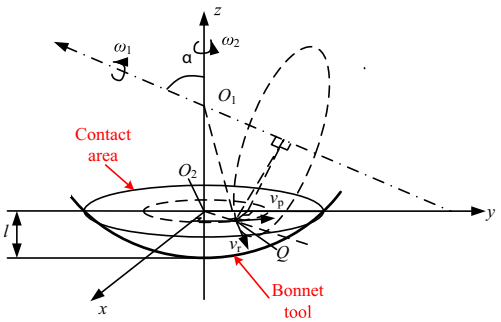

Fig. 2 Schematic diagram of the precession bonnet tool

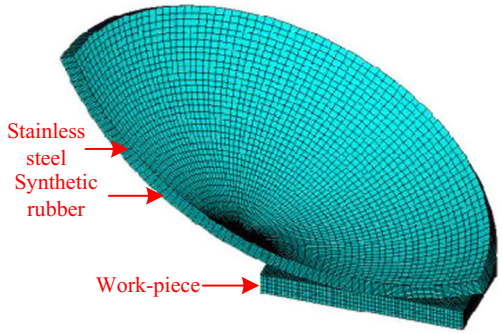

Fig. 3 FEA model

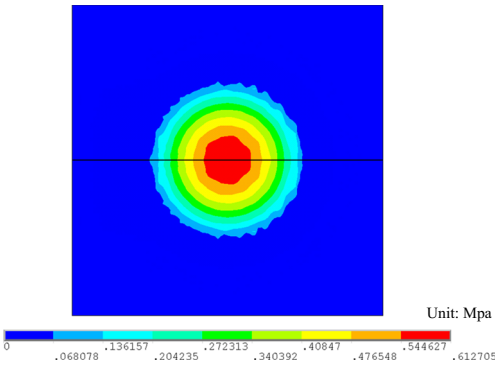

Fig. 4 Simulated pressure distribution of the polishing area

center of the bonnet tool, O_2 is the center of the contact area, l is the Z offset of the bonnet, and α is the precession angle.

The total relative speed of $Q(x, y)$ can be expressed as follows:

$$v_Q = v_r + v_p \tag{2}$$

$$v_r = \omega_1 \times l_{O_1Q} = \begin{pmatrix} |\omega_1|[(R-l)\sin\alpha - y\cos\alpha] \\ |\omega_1| x\cos\alpha \\ |\omega_1| x\sin\alpha \end{pmatrix}^T \tag{3}$$

$$v_p = \omega_2 \times l_{O_1Q} = \begin{pmatrix} -|\omega_2| y \\ |\omega_2| x \\ 0 \end{pmatrix}^T \tag{4}$$

where R is the radius of the bonnet.

Deduced from Eqs. (2), (3), and (4),

$$v_Q = \left[(v_{rx} + v_{px})^2 + (v_{ry} + v_{py})^2 \right]^{\frac{1}{2}} = \left\{ \begin{array}{l} [|\omega_1|(R\sin\alpha - l\sin\alpha - y\cos\alpha) - |\omega_2| y]^2 \\ +(|\omega_1|\cos\alpha + |\omega_2|)^2 x^2 \end{array} \right\}^{\frac{1}{2}} \tag{5}$$

2.2 Analysis of the pressure distribution in the contact area based on FEA

Due to the reason that pressure distribution in the contact area is difficult to extract through the experiment, a finite element model to simulate the BP process is established. Figure 3 shows the FEA model. Half of the polishing model is used to simplify the procedure and improve the solution efficiency. In the actual polishing process, there are polishing slurry between the tool and the workpiece, and the elastohydrodynamic film thickness and the film pressure of the slurry could impact the contact pressure [19]. However, it is too complicated to consider this in the model of FEA, and it is usually ignored in the FEA model [6, 20]. To simplify the simulation model, just the spherical part of the bonnet tool is used, and the polishing pad is ignored here [6]. The bonnet tool has two layers, which are synthetic rubber layer and stainless steel layer, respectively. The radius of the bonnet tool is 80 mm. The workpiece is BK7 whose dimension is 50×50×5 mm. The inflated pressure is 0.25 MPa. The precession angle is 23° and Z offset is 1 mm. Table 1 shows the material characters of materials used in the FEA model.

Table 1 Material characteristic for modeling

Material	Density (g/cm^3)	*Young's modulus* (MPa)	Poisson's ratio
Synthetic rubber	0.95	1.5	0.47
Stainless steel	7.30	1.9E+5	0.26
BK7	2.53	8.1E+4	0.21

The obtained simulation result was shown in Fig. 4. The pressure in the contact area distributes like a Gaussian shape. It is the largest in the center and gradually decreases toward the edge. This is coincident with the pressure distribution proposed by Kim et al. [18], of which the stress distribution of the bonnet polishing contact areas can be expressed as a modified Gaussian function:

$$p_S = p_{\max}\left[\exp\left(-\frac{\lambda^2}{2\sigma^2}\right)\right]^{\varphi} \tag{6}$$

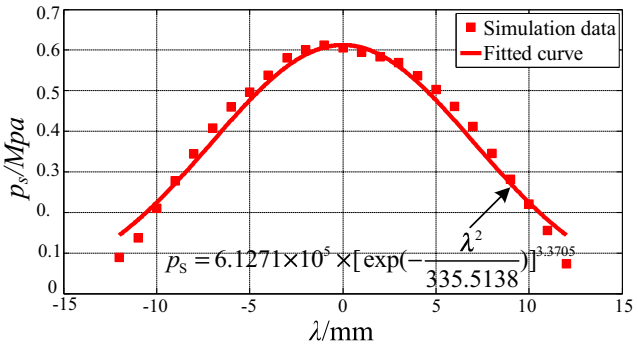

Fig. 5 Fitted results of the simulation data

(a) Four different directions of the tilted bonnet tool

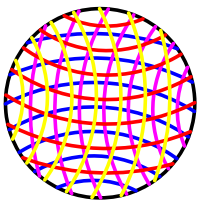

(b) Polished mark

Fig. 6 Movement of four-step tilted polishing. **a** Four different directions of the tilted bonnet tool. **b** Polished mark

where p_{max} is the maximum pressure in the contact area, λ is the distance from one of the point in the contact area to the center, σ is the standard deviation, and φ is the modification coefficient.

In order to obtain the pressure data in the contact area, the data was extracted along the black line as shown in Fig. 4. The least-square method is used to fit the simulation data according to Eq. (6). Figure 5 shows the fitting result. It can be seen that the fitted curve fits the simulation data well. Hence, the function shown in Fig. 5 could be used to determine the pressure distribution in the contact area.

2.3 Three kinds of models of sTIF

Theoretically, continuous precession polishing movement is preferable to be used and can achieve the best texture of the part surface. However, due to the difficulty to implement

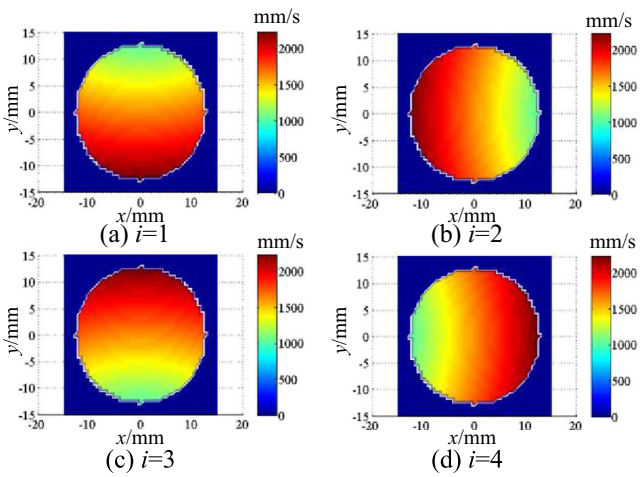

Fig. 7 Polishing velocity distribution in the contact area (n_1=500 rpm, ω_1=2πn_1/60, R=80 mm, l=1 mm, α=23°)

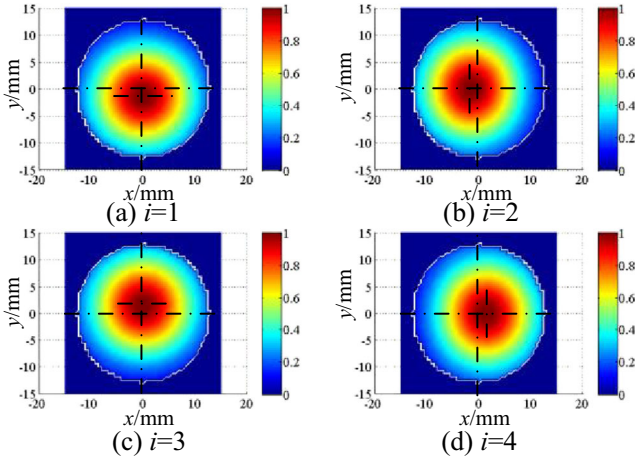

Fig. 8 Simulation results of the normalized $sTIF_t$ (n_1=500 rpm, ω_1=2πn_1/60, R=80 mm, l=1 mm, α=23°)

continuous precession movement, discrete precession movement is usually used for instead, and in the pre-polishing process, only tilted polishing (v_p=0) is needed in most cases. Hence, sTIFs of these three kinds of movement styles are needed to be modeled.

As the pressure distribution of the polishing area is constant during the polishing process, combining Eqs. (1), (5), and (6), the material removal amount of static tool influence function of continuous precession polishing ($sTIF_c$) in dwell time (T) can be expressed as follows:

$$\mathrm{sTIF_c}(x,y) = kp\int_0^T v_Q dt = kp_{\max}\left[\exp\left(-\frac{(x^2+y^2)}{2\sigma^2}\right)\right]^{\varphi} \int_0^T \left\{\begin{array}{l}[|\omega_1|(R\sin\alpha - l\sin\alpha - y\cos\alpha) - |\omega_2|y]^2 \\ +(|\omega_1|\cos\alpha + |\omega_2|)^2 x^2\end{array}\right\}^{\frac{1}{2}} dt \quad (7)$$

The continuous precession is hard to control practically, especially for polishing aspheric lenses, several steps of tilted

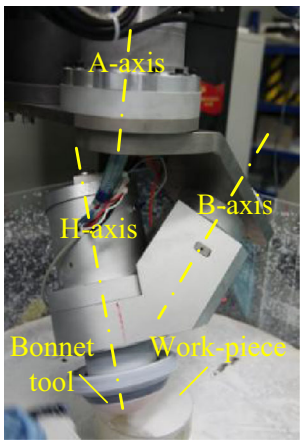

Fig. 9 Experimental prototype of BP process

Table 2 Polishing conditions

	Spot 1	Spot 2	Spot 3
Inner pressure (p) (MPa)	0.25	0.25	0.25
H-axis speed (n_1) (rpm)	500	500	500
A-axis speed (n_2) (rpm)	20	0	0
Tool Z offset (l) (mm)	1	1	0.35
Precession angle (α) (°)	23	23	23
Dwell time (T) (s)	12	4×3[a]	6

[a] Four-step tilted polishing, each step takes 3 s

polishing in different directions are used instead [3] which also called N-step discrete precession polishing. Figure 6 shows the movement of four-step tilted polishing. Figure 6a shows four different directions of the tilted bonnet tool during the four-step tilted polishing. The polished mark generated in the contact area under the four-step tilted polishing is shown in Fig. 6b.

In tilted polishing, of which ω_2=0, the material removal amount of static tool influence function of tilted polishing ($sTIF_t$) in dwell time (T) can be expressed as follows:

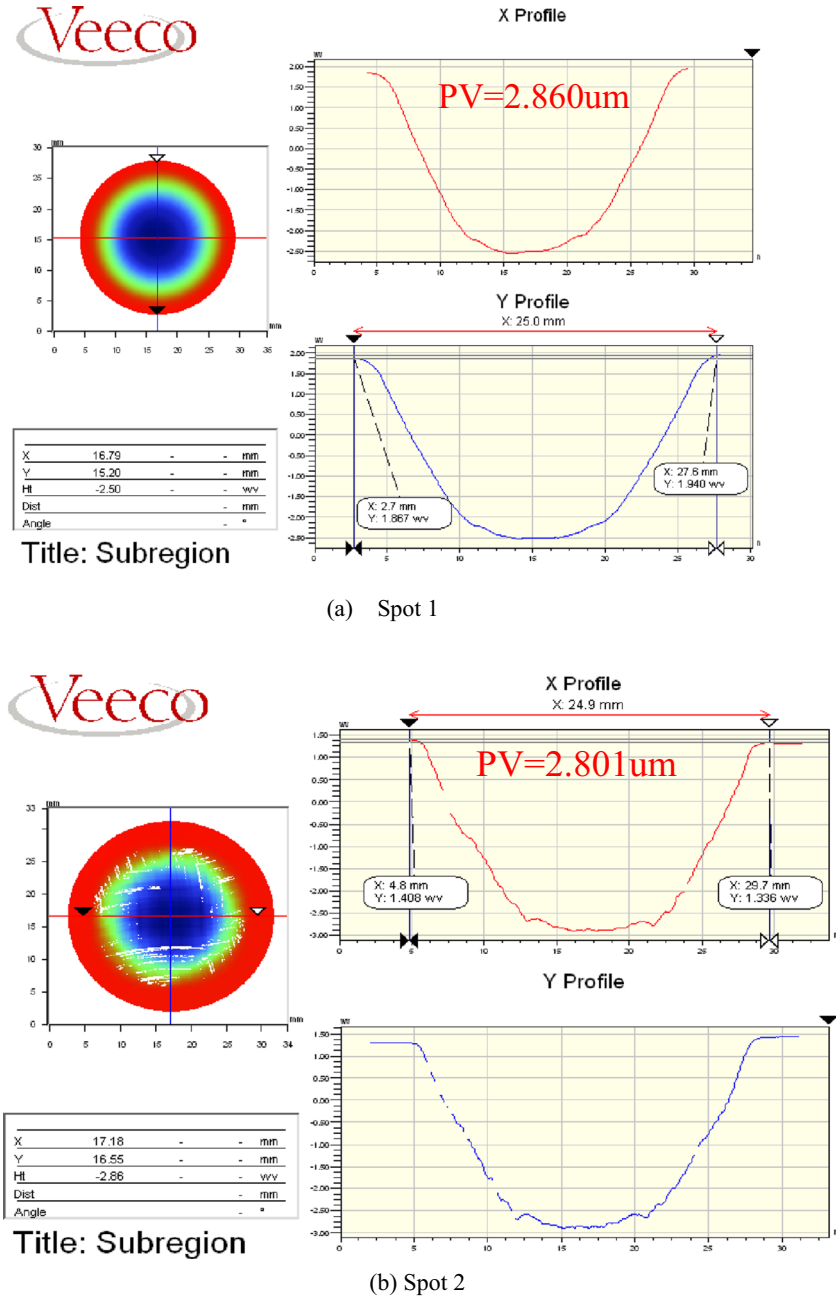

Fig. 10 Contour of the polishing spot. **a** Spot 1. **b** Spot 2

(a) Spot 1

(b) Spot 2

$$\mathrm{sTIF}_t(x,y) = kp_{\max}\left[\exp\left(-\frac{(x^2+y^2)}{2\sigma^2}\right)\right]^{\varphi} \left\{\begin{array}{l}[|\omega_1|(R\sin\alpha - l\sin\alpha - y\cos\alpha)]^2 \\ +(|\omega_1|\cos\alpha)^2x^2\end{array}\right\}^{\frac{1}{2}} T \quad (8)$$

For N-step discrete precession polishing, the direction of the velocity distribution changes step by step. The dwell time for each step is T/N, then the material removal amount of static tool influence function of discrete precession polishing ($\mathrm{sTIF_d}$) can be expressed as follows:

$$\mathrm{sTIF_d}(x,y) = kp_{\max}\left[\exp\left(-\frac{(x^2+y^2)}{2\sigma^2}\right)\right]^{\varphi} \left\{\begin{array}{l}[|\omega_1|(R\sin\alpha - l\sin\alpha - y\cos\alpha)]^2 \\ +(|\omega_1|\cos\alpha)^2x^2\end{array}\right\}^{\frac{1}{2}} \sum_{i=1}^{N} \Delta_i \frac{T}{N} \quad (9)$$

where Δ_i is the matrix of the velocity direction of each step.

Assuming that the initial velocity direction angle is zero, the velocity direction angle of the ith step (θ_i) can be expressed as follows:

$$\theta_i = (i-1)\cdot\frac{360}{N} \quad (10)$$

Using the four-step tilted polishing, the polishing velocity distribution in the contact area is demonstrated in Fig. 7. Figure 7a shows the velocity distribution according to the tool tilted direction showed in Fig. 2. It is symmetric in the x-direction but gradually increases along the negative direction of y-axis. This is due to that along the negative direction of y-axis, the further it is from the axis of H-axis and the larger the corresponding linear velocity. Figure 7b, c, and d are the corresponding polishing velocity distribution when the bonnet tool rotates clockwise 90°, 180°, and 270° on the basis of the initial direction, respectively. It can be observed from Fig. 7 that, with the change in the direction of the bonnet tool, the velocity distribution of the polishing area changes correspondingly.

In order to observe the distribution of the influence functions under different polishing directions, Eq. (8) is used to simulate $\mathrm{sTIF_t}$. The simulation results are normalized as shown in Fig. 8, as the removal coefficient has not been determined here. Comparing Fig. 8 with Fig. 7, it is interesting to note that the asymmetric distribution of the velocity leads to the asymmetric distribution of the corresponding influence function. Each peak of the removal function deviates from the center, and the direction of the deviation is the same as the direction which the velocity increases along with.

3 Experimental device and conditions

In order to determine the value of the removal coefficient (k), and to verify the simulation results, an experimental prototype for BP has been designed as shown in Fig. 9. A group of the polishing spot experiments are conducted on BK7 workpiece. The initial PV value of the surface is smaller than 0.1λ (λ= 632.8 nm), which is well suited for the extraction of the polishing spot. R80 bonnet is selected and cerium oxide slurry is used whose weight percentage is 5.5 %. The material of the polishing pad is polyurethane. Other detailed polishing conditions are demonstrated in Table 2. The experiment totally extracts three spots, which are $\mathrm{sTIF_c}$, $\mathrm{sTIF_d}$, and $\mathrm{sTIF_t}$, respectively.

4 Results and discussion

Figure 10 shows the contours of the generated polishing spot 1 and spot 2. Figure 10a is the contour of the extracted $\mathrm{sTIF_c}$, which is almost a standard Gaussian-like shape. The $\mathrm{sTIF_d}$ is shown in Fig. 10b, which is also a Gaussian-like shape but with obvious polishing mark in four directions. There are missing data in some region because of the too large wave front gradient there. In addition, since the center of the bonnet tool slightly deviated from the A-axis in the experimental prototype, the center of polishing area in each step did not coincide. It leads to some protrusions in four directions after overlapping.

In order to extract the complete data of the tilted polishing spot, the polishing time is shortened to 6 s in the third polishing spot extraction experiment, and tool Z offset reduces to 0.35 mm. Figure 11 shows the extracted contour of spot 3. It can be seen that the tilted polishing spot has obvious mark of removal, and the shape of the contact area is ellipse. This may be due to the property of rubber.

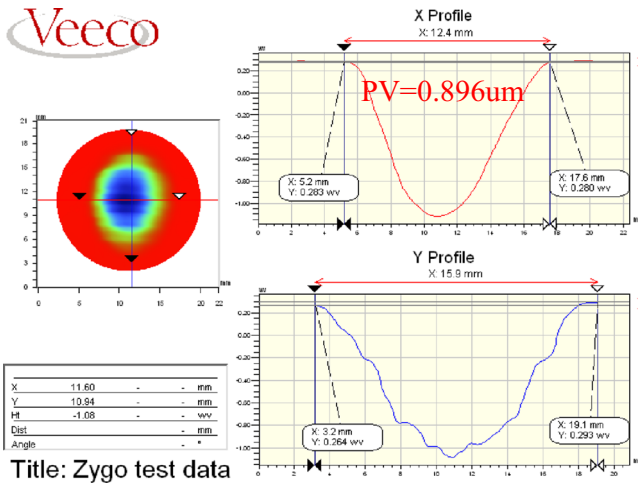

Fig. 11 Contour of the tilted polishing spot (spot 3)

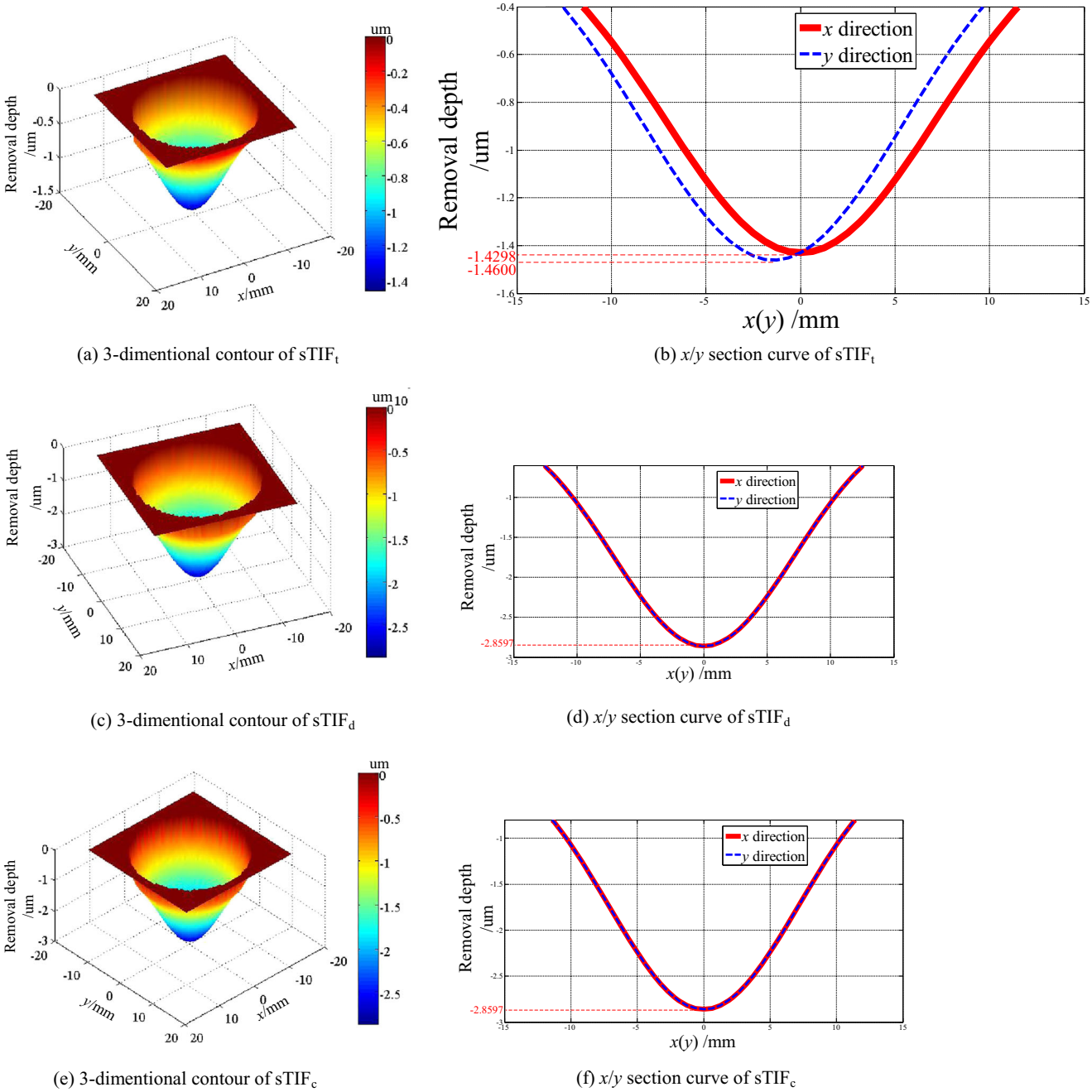

(a) 3-dimentional contour of $sTIF_t$

(b) x/y section curve of $sTIF_t$

(c) 3-dimentional contour of $sTIF_d$

(d) x/y section curve of $sTIF_d$

(e) 3-dimentional contour of $sTIF_c$

(f) x/y section curve of $sTIF_c$

Fig. 12 Simulation results of three kinds of sTIF. **a** Three-dimensional contour of $sTIF_t$. **b** x/y section curve of $sTIF_t$. **c** Three-dimensional contour of $sTIF_d$. **d** x/y section curve of $sTIF_d$. **e** Three-dimensional contour of $sTIF_c$. **f** x/y section curve of $sTIF_c$

According to the above experimental results, it is shown that the removal depth of $sTIF_c$ and $sTIF_d$ are almost the same, which are 2.801 and 2.860 μm, respectively. The functions of the pressure distribution and the polishing velocity have been proposed in part 2, and the removal coefficient (k) can be determined based on the PV value of the polishing spot:

$$k = \frac{\max(\mathrm{sTIF_c})}{\max(p \cdot v)} \tag{11}$$

where $\max(sTIF_c)$ is the PV value of the polishing spot generated under the condition as shown in Table 2, $\max(p \cdot v)$ is the maximum value calculated according to Eqs. (5) and (6). As a result, the value of k is -2.4059×10^{-13}. The simulation of $sTIF_c$, $sTIF_d$, and $sTIF_t$ could be carried out based on Eqs. (7), (8), and (9), which have been demonstrated in Fig. 12.

Figure 12a, b are the simulation results of $sTIF_t$, which are three-dimensional contour of $sTIF_t$ and x/y section curve of $sTIF_t$, respectively. It is noted that the shape of $sTIF_t$ is not rotating axisymmetric. The x section curve and y section curve

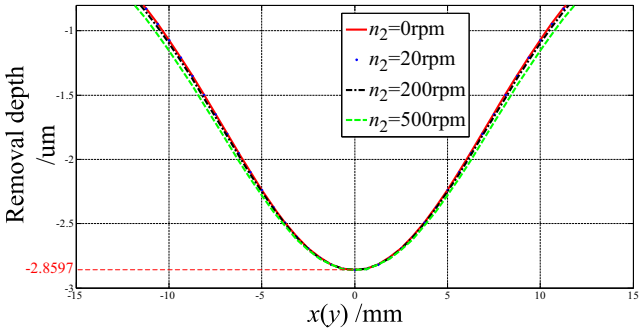

Fig. 13 x section curve of $sTIF_c$ under different rotation speed of A-axis

do not coincide. It is induced by the asymmetric distribution of the polishing velocity. Figure 12c, d and e, f, respectively, shows three-dimensional contour and x/y section curve of $sTIF_d$ and $sTIF_c$. By comparison, it can be found that both $sTIF_d$ and $sTIF_c$ are standard modified Gaussian-like shape and rotating axisymmetric. This confirms the experimental results in Fig. 10. Thus, it verifies the accuracy of the sTIF model and also proves the necessity of the precession movement.

In order to further explain the difference between $sTIF_d$ and $sTIF_c$, the comparison of x-direction section curve of them has been made. The other two $sTIF_c$ are added in, of which A-axis rotation speed n_2 is 200 rpm and 500 rpm, to analyze the effect of A-axis rotation speed on sTIF. The results are shown in Fig. 13.

Figure 13 shows the x section curve of $sTIF_c$ under different rotation speed of A-axis. n_2=0 rpm and n_2=20 rpm correspond to the aforementioned $sTIF_d$ and $sTIF_c$. It is found that the removal distributions of these four influence functions are quite similar. Hence, the rotation speed of A-axis does not have significant effect on sTIF. Besides, the maximum removal depths of these four influence functions are the same. The reason is that A-axis went through the center of the contact area, and it does not affect the polishing velocity of the center point. From the center to the edge, the effect of the rotation speed of A-axis increases. This is mainly because the velocity derived from the A-axis rotation at the edge is larger than that at the center.

5 Conclusions

Three kinds of sTIF are mathematically modeled combining the geometric model with FEA in this paper, which are $sTIF_t$, $sTIF_d$, and $sTIF_c$, respectively. Simulation analysis and experiments were also conducted to verify these models, and the following conclusions were made based on the obtained results:

1. The polishing velocity distribution is inclined to one direction, the point with the farther distance from the H-axis, the larger velocity it would be, and the changing direction is directly related to the rotating angle of A-axis.
2. The pressure distribution in the contact area is a Gaussian-like shape with a proper Z offset of the bonnet tool. Induced by the inclined distribution of the velocity distribution, the shape of $sTIF_t$ is asymmetric. The peak of $sTIF_t$ deviates from the center, and the direction of the deviation is the same as the direction which the velocity increases along with.
3. The rotation speed of A-axis has few effects on sTIF. It can be ignored in the practical machining process, and the continuous precession polishing could be replaced by discrete precession polishing for the ease of control especially when polishing aspheric surfaces.

Acknowledgments We appreciate the invaluable expert comments and advices on the manuscript from all anonymous reviewers. This work is supported by major national science and technology projects (no. 2013ZX04006011-206)

References

1. Bingham RG, Walker DD, Kim DH, Brooks D, Freeman R, Riley D (2000) Novel automated process for aspheric surfaces. Proc SPIE 4093:281–289
2. Walker DD, Beaucamp A, Brooks D, Doubrovski V, Cassie M, Dunn C, Freeman R, King A, Libert M, McCavana G, Morton R, Riley D, Simms J (2004) Recent development of precessions polishing for larger components and free-form surfaces. Proc SPIE 5523:445–448
3. Walker DD, Brooks D, King A, Freeman R, Morton R, McCavana G, Kim SW (2003) The 'precessions' tooling for polishing and figuring flat, spherical and aspheric surfaces. Opt Express 11(8):958–964
4. Walker DD, Freeman R, Morton R, McCavana G, Beaucamp A (2006) Use of the 'precessions' ™ process for prepolishing and correcting 2D & 2½D form. Opt Express 14(24):11787–11795
5. Walker DD, Yu G, Li H, Messelink W, Evans R, Beaucamp A (2012) Edges in CNC polishing: from mirror-segments towards semiconductors, paper 1: edges on processing the global surface. Opt Express 20(18):19787–19798
6. Li H, Walker DD, Yu G, Sayle A, Messelink W, Evans R, Beaucamp A (2013) Edge control in CNC polishing, paper 2: simulation and validation of tool influence functions on edges. Opt Express 21(1): 370–381
7. Jones RA (1986) Computer-controlled optical surfacing with orbital tool motion. Opt Eng 25(6):785–790
8. Allen LN, Romig HW (1990) Demonstration of an ion figuring process. Proc SPIE 1333:22–33
9. Jiao C (2008) Study on the material removal mechanisms and fundamental processes for ion beam figuring optical mirrors. Dissetation, National University of Defense Technology
10. Dai Y, Song C, Peng X, Shi F (2010) Calibration and prediction of removal function in magnetorheological finishing. Appl Opt 49(3): 298–306
11. Kordonski W, Jacobs S (1996) Magnetorhelogical finishing. Int J Mod Phys B 10:2837–2848
12. Fähnle OW, Brug H, Frankena HJ (1998) Fluid jet polishing of optical surfaces. Appl Opt 37(28):6671–6673

13. Shiou FJ, Loc PH, Dang NH (2013) Surface finish of bulk metallic glass using sequential abrasive jet polishing and annealing processes. Int J Adv Manuf Technol 66(9–12):1523–1533
14. Tsai FC, Yan BH, Kuan CY, Hsu RT, Hung JC (2009) An investigation into superficial embedment in mirror-like machining using abrasive jet polishing. Int J Adv Manuf Technol 43(5–6): 500–512
15. Yang L (2001) Advanced technology of optics manufacturing. Science Press, Beijing
16. Lin TR (2007) An analytical model of the material removal rate between elastic and elastic-plastic deformation for a polishing process. Int J Adv Manuf Technol 32(7–8):675–681
17. Yi HS, Yang HS, Lee YW, Kim SW (2011) Kernel TIF method for effective material removal control in rotating pitch tool-based optical figuring. Int J Adv Manuf Technol 55(1–4):75–81
18. Kim DW, Kim SW (2005) Static tool influence function for fabrication simulation of hexagonal mirror segments for extremely large telescope. Opt Express 13(3):910–917
19. Mittal R, Singh R, Joshi SS (2012) Elastohydrodynamic lubrication modeling of hydrodynamic nanopolishing process. J Manuf Sci Eng 134(4):041001–041011
20. Kim DW, Park WH, Kim SW, Burge JH (2009) Parametric modeling of edge effects for polishing tool influence functions. Opt Express 17(7):5656–5665